J Appl Electrochem (2012) 42:249–255
DOI 10.1007/s10800-012-0391-7

ORIGINAL PAPER

Synthesis and characterization of carbon aerogels doped with the anatase form of titanium oxide

Xingchao Li · Ling Liu · Qinghan Meng · Bing Cao

Received: 13 December 2011 / Accepted: 6 February 2012 / Published online: 17 February 2012

Abstract TiO_2-doped carbon aerogels (CAs) were synthesized by sol–gel polymerization of a mixture of resorcinol, formaldehyde and tetrabutyl orthotitanate, followed by gelation and supercritical drying and carbonization in N_2 gas atmosphere. The morphology of these TiO_2-doped CAs was characterized by transmission electron microscopy. X-ray diffraction and Brunauer–Emmett–Teller methods were employed to determine the microstructure and surface characteristics of samples. It was found that the doped TiO_2 had no significant effect on the surface area of the samples, whereas the pore and mesopore volumes were increased by the addition of TiO_2. The TiO_2 particles were kept still as anatase in samples carbonized at 900 °C, and did not transform into rutile on heating. Electrochemical performance of the samples as electrode materials was studied by cyclic voltammetry, electrochemical impedance spectroscopy, and constant current charge/discharge measurements. The results showed that the specific capacitance of CA electrodes had been improved by TiO_2 doping, and the samples with wider pore diameters have higher capacitance values.

Keywords Carbon aerogels · Tatania doping · Anatase

1 Introduction

Carbon aerogels (CAs) are among the most promising materials for use as electrodes in an electrical double-layer capacitor (EDLC) [1–3] because of its interconnected three-dimensional network structure, high specific surface area, good electrical conductivity, and suitable pore size distribution for common electrolytes. CAs were prepared via the sol–gel polycondensation of certain organic monomers, such as resorcinol with formaldehyde. This method was first described by Pekala [3–6]. The porous sol–gel materials can be modified through the introduction of various doped molecules that can alter the structure and physical properties of the materials. Metal-doped CAs have recently been synthesized through the addition of metal salt during the sol–gel polymerization reaction with the goal of modifying the properties and expanding the potential application of the aerogel [7–23].

Among these metals, titania (TiO_2) is a material of great interest. TiO_2 is generally used in photocatalytic air, water purification, and photocatalysis of organic pollutants [24–29]. Moreover, the incorporation of TiO_2 into activated carbon has been shown to have a synergistic effect on the photodegradation of phenol and other model compounds [30, 31]. Moreno [32] prepared a TiO_2/carbon composite using the sol–gel method. Results showed that the meso- and macroporosity, as well as the surface area, depended on TiO_2 content and heat treatment. The metal oxide phase essentially occurred as either anatase in samples prepared at 500 °C or as a mixture of anatase and rutile in those prepared at 900 °C.

In this study, TiO_2-doped CAs were synthesized by introducing TiO_2 in the sol–gel process of the resorcinol–formaldehyde polymer precursors. The TiO_2 particles were maintained as anatase in samples carbonized at 900 °C and did not transform into rutile on heating. The aim of the current research was to develop optimum methods for synthesizing CAs with fine, well-dispersed TiO_2 particles. This effect is expected to be a potential material for EDLC.

X. Li · L. Liu · Q. Meng (✉) · B. Cao (✉)
College of Materials Science and Engineering,
Beijing University of Chemical Technology,
Beijing 100029, China
e-mail: qhmeng@mail.buct.edu.cn

B. Cao
e-mail: bcao@mail.buct.edu.cn

The microstructure of these TiO_2-doped CAs was characterized by nitrogen adsorption/desorption analysis, X-ray photoelectron spectroscopy (XPS), X-ray diffraction (XRD), and transmission electron microscopy (TEM). The electrochemical behavior of the sample as electrode materials in EDLCs was investigated by cyclic voltammetry (CV), electrochemical impedance spectroscopy (EIS), and constant current charge/discharge test.

2 Experimental

2.1 Preparation of TiO_2-doped CA

Ethanol (E) was selected as the solvent instead of water because tetrabutyl titanate is hydrolyzed in water, but is soluble in ethanol. Initially, resorcinol and formaldehyde were dissolved in E with a molar ratio of 1:2 in a 40 mL of solution. Tetrabutyl orthotitanate (TBTi) was dissolved in ethanol (the stoichiometric TBTi/E volume ratio was 1:1) and added drop by drop to the above solution by maintaining a temperature of 50 °C with continuous magnetic stirring. The mixture was then aged for 5 d at 70 °C to obtain wet gel. The wet gel was washed with acetone until the water was completely exchanged and then dried with supercritical petroleum ether ($T_c = 250$ °C, $P_c = 7.5$ MPa). Carbonization of the TiO_2-doped organic aerogels was performed at 900 °C for 2 h under an N_2 atmosphere. The synthesis conditions of different samples are presented in Table 1.

2.2 Characterization of TiO_2-doped CAs

Surface area and pore volume were determined by a Sorptomatic 1990 with samples heated to 200 °C under vacuum (10^{-5} Torr) for 2 h to remove all adsorbed species. The nitrogen adsorption data were taken at 77 K to calculate the surface area using the Brunauer–Emmett–Teller (BET) model. The average pore diameter D was computed as $4V_{TOTAL}/S_{BET}$.

Thermal gravimetric analysis (TGA) of the TiO_2-doped CA was performed using a TG-209C TGA instrument (Netzsch). The samples were heated in nitrogen from 30 °C to 900 °C (flow rate = 75 mL min^{-1}) with a heating rate of 10 °C min^{-1}.

The surface elements were analyzed using an X-ray photoelectron spectrometer (ThermoFisher, ESCALab 250) with an Al Kα radiation source (1486.6 eV) to excite the photoelectrons in an ultra-vacuum atmosphere at $\sim 10^{-9}$ Torr.

XRD patterns for CA powders were obtained using a D/Max 2500 diffractometer (40 kV and 200 mA) using Cu Kα radiation, performed in the 2θ range of 5° to 90° at a scan rate of 10° min^{-1}.

TEM of the TiO_2-doped CAs was performed on an H-800 instrument operating at 200 keV.

Table 1 Synthesis conditions of the CAs

Sample	R (mol)	F (mol)	The solution of TBTi dissolved in ethanol (mL)	TiO_2 content (wt%)
CA-0	0.055	0.11	0	0
CA-1	0.055	0.11	5	12
CA-2	0.055	0.11	10	20
CA-3	0.055	0.11	15	31
CA-4	0.030	0.06	10	23

2.3 Electrochemical measurements

The carbon electrodes were prepared by mixing the CAs with acetylene carbon black and polytetrafluoroethylene with a weight ratio of 75:20:5. The samples were dried for 8 h at 80 °C and then pressed to form a thick film. Pieces of the film with a radius of approximately 7.5 mm and weight of approximately 15–30 mg were then pressed onto nickel foam.

A unit cell for a capacitor was fabricated with two electrodes separated by a thin polypropylene film in 30% KOH aqueous solution as electrolyte (Fig. 1). CV experiments were realized using an electrochemical station (Zahner-Electrik, Germany) in the potential range of 0–1.0 V. In the CV experiments, carbon electrode was used as a working electrode, whereas platinum and calomel electrode was used as a counter and reference electrode, respectively. EIS measurements were taken at ambient temperature in a frequency range between 50 kHz and 10 MHz using a frequency response analyzer (Zahner-Electrik, Germany).

The constant current charge/discharge experiments were conducted in a current range of 2–10 mA at room temperature using a LAND battery tester (Wuhan Jinnuo Instruments, China). The specific capacitance was calculated from the slope of the discharge.

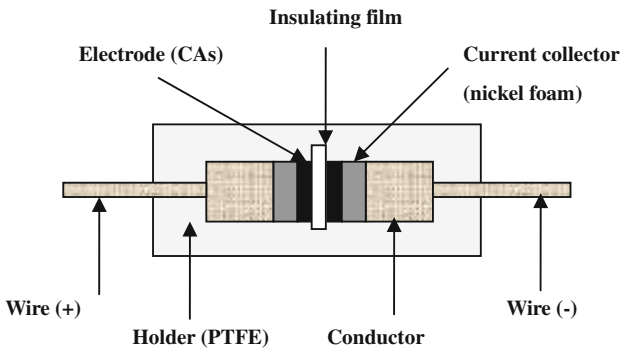

Fig. 1 Schematic diagram of the capacitor

3 Results and discussion

3.1 Structure characteristics of CAs

Table 2 shows the surface area and porosity of TiO_2-doped CAs. The surface area (S_{BET}) of aerogels falls between 502 and 552 $m^2\ g^{-1}$, indicating that the incorporation of TiO_2 has minimal effect on the surface area. All the aerogels have higher volumes of mesopore than micropore, with a mesopore volume ranging from 0.39 to 0.76 $cm^3\ g^{-1}$. TiO_2 was observed to increase both mesopore and pore volume. This result is ascribed to the fact that tetrabutyl titanate acts as a catalyst for the regulation of pore structure. However, excessive tetrabutyl titanate facilitates the rapid formation of the gel network, resulting in the collapse of some pores. Therefore, the mesopore and pore volumes of sample CA-3 (0.52 and 0.56 $cm^3\ g^{-1}$, respectively) were slightly higher than those of sample CA-0 (0.39 and 0.48 $cm^3\ g^{-1}$).

Figure 2 shows the pore size distributions of the TiO_2-doped CAs. The pore size distribution is calculated from the adsorption branch of the isotherm using the Barrett–Joyner–Halendar method. The results exhibit single pores with the most probable pore size in the range of 3.8–10.5 nm. Therefore, compared with sample CA-0, the average pore size, mesopore volume, and pore volume can be increased by incorporating TiO_2 or decreasing the solid ratio in the E solvent. Particularly, the sample CA-2 significantly increases the average pore size and mesopore volume.

Table 2 Surface area and porosity analysis of CAs

Sample	S_{BET} ($m^2\ g^{-1}$)	Mesopore volume ($cm^3\ g^{-1}$)	Pore volume ($cm^3\ g^{-1}$)	D (nm)
CA-0	502	0.39	0.48	3.8
CA-1	519	0.65	1.02	7.9
CA-2	528	0.76	1.38	10.5
CA-3	537	0.52	0.56	4.2
CA-4	552	0.70	1.12	8.1

3.2 Morphology characteristics of CAs

Figure 3 shows the weight loss curve of samples CA-0 and CA-2. The first stage is 30–300 °C, which can be attributed to the loss of adsorbed water and acetone. The next stage is 300–500 °C, wherein the samples continued to lose the low molecule matter, in addition to the precipitation of H_2, CO_2, and CH_4. This stage, which is followed by the loss of O_2 and CO_2, facilitates the formation of TiO_2 [33]. Two curves have significant differences at the final stage. The upper curve (sample CA-2) decelerates the rate of weight loss. This finding may be attributed to the production of crystalline TiO_2, which prevents the continuous weight loss of carbon. The final mass loss of CA-2 was 37.39%, significantly less than that of sample CA-0. The sample had almost no weight loss after 850 °C; hence, the carbonization temperature was confirmed as 900 °C.

The XPS patterns of sample CA-2 are shown in Fig. 4, confirming that titanium was doped in CAs. The chemical composition of the sample surfaces can be identified by the survey scan spectra. Figure 5 shows the XPS analysis of the Ti-2*p* orbital of sample CA-2. The oxidation state of titanium can be assessed based primarily on the energy difference between 1/2 and 3/2 shells of titanium. The peak of Ti-2*p* comprised Ti2*p* 1/2 at 464 eV and Ti2*p* 3/2 at 458 eV, consistent with the binding energy of Ti^{4+}.

The XRD patterns of samples CA-0, CA-1, and CA-2 are shown in Fig. 6. Sample CA-0 was characterized by only the carbon phase, showing two peaks at approximately 23° and 43.5°, which correspond to the (002) and (100) graphite diffraction peaks. Compared with that of sample

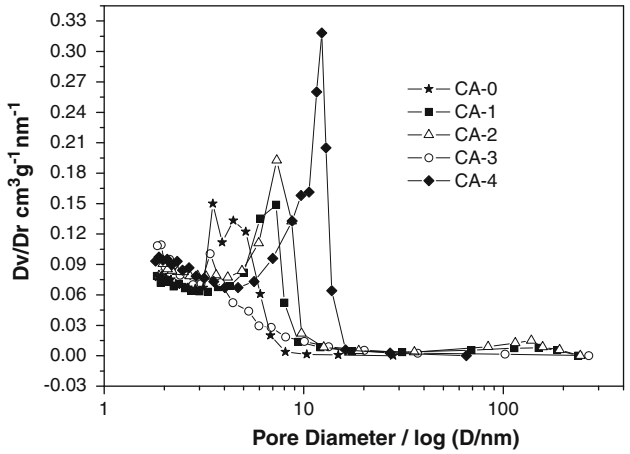

Fig. 2 Pore size distribution of TiO_2-doped carbon aerogels

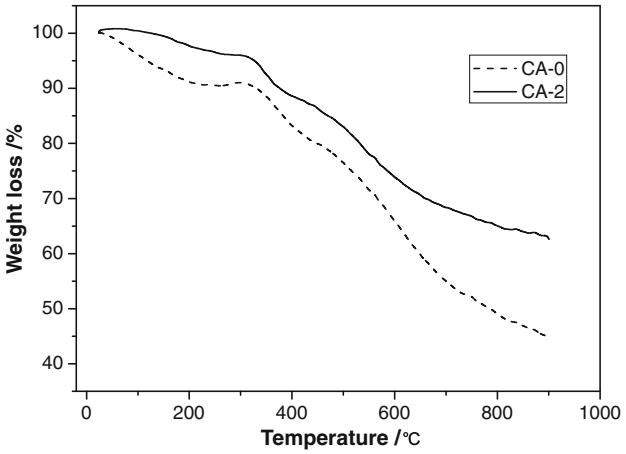

Fig. 3 TG analyses of TiO_2-doped carbon aerogels

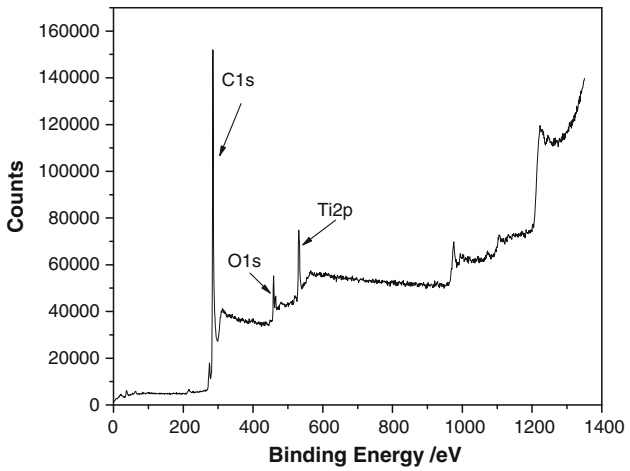

Fig. 4 XPS analysis of sample CA-2

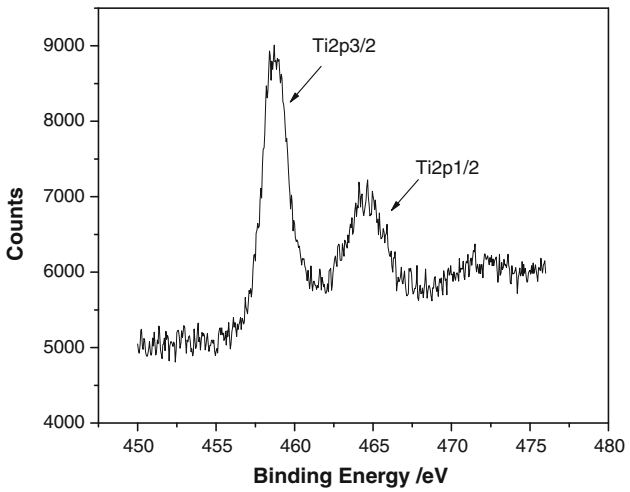

Fig. 5 XPS Ti2*p* of sample CA-2

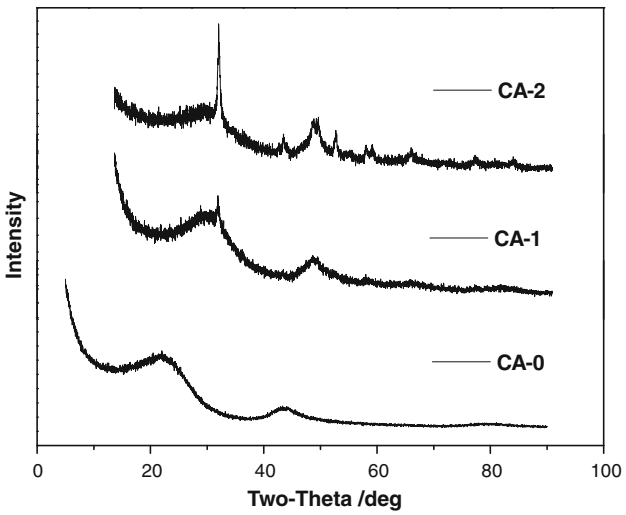

Fig. 6 XRD patterns of sample CA-0, CA-1, and CA-2

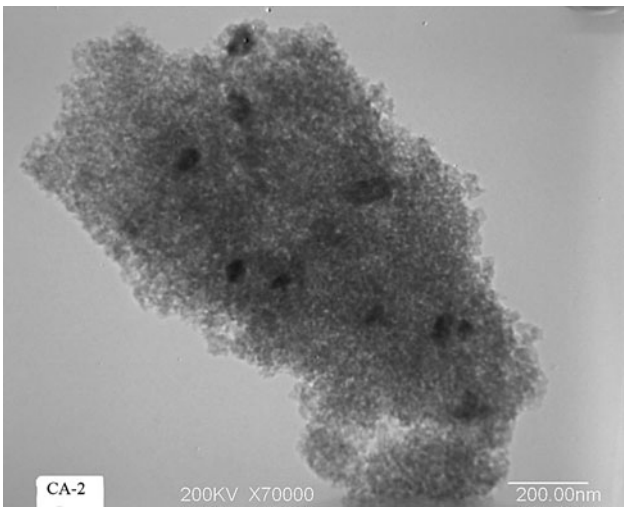

Fig. 7 TEM images of CA-2

CA-2, the TiO_2 peak of sample CA-1 was not obtained, which may be attributed to lower TBTi content. The XRD patterns of the sample show that the 002 diffraction peak is similar in samples CA-0 and CA-2, whereas the 100 diffraction peak is narrower and sharper in sample CA-2 than in sample CA-0. These findings indicate that TiO_2 catalyzed the partial graphitization of the CA structure. The partial graphitization of the CA structure improves the conductivity of materials.

Sample CA-2 was apart from the carbon peak, in addition to the titanium peak, by only the anatase phase identified at $2\theta = 25.28°$ for (101) and 48.05° for (200). Anatase is a metastable polymorphic form of TiO_2 and transforms into rutile on heating. For pure oxides, the transformation is very rapid at temperatures above 730 °C [34]. The phase transition temperature has been shown to depend on impurity content, particle size, and surface area. Sample CA-2 was carbonized at 900 °C, but the main diffraction peaks of rutile did not appear in Fig. 6. The result is different from that previously reported [32]. This result may be attributed to the diffusion of TiO_2 into the CA lattice, which has changed the phase transition temperature.

The TiO_2 dispersion in CA samples was analyzed by TEM. The TEM image of sample CA-2 shown in Fig. 7 indicates that the TiO_2 nanoparticles are well distributed and that the average particle size of the TiO_2 is $\sim$20 nm.

3.3 Electrochemical properties

The cyclic voltammogram curves of the CA-2 sample at different scan rates are depicted in Fig. 8. The redox effect in the potential range was not observed, and all curves show the typical capacitor with symmetric cyclic rectangular shapes, indicating that the charging/discharging

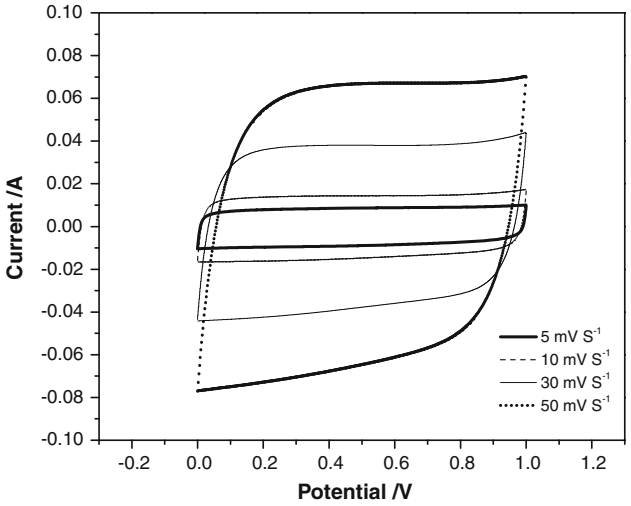

Fig. 8 Cyclic voltammograms of the CA-2 samples measured at 5–50 mV s^{-1} in 30% KOH aqueous solution

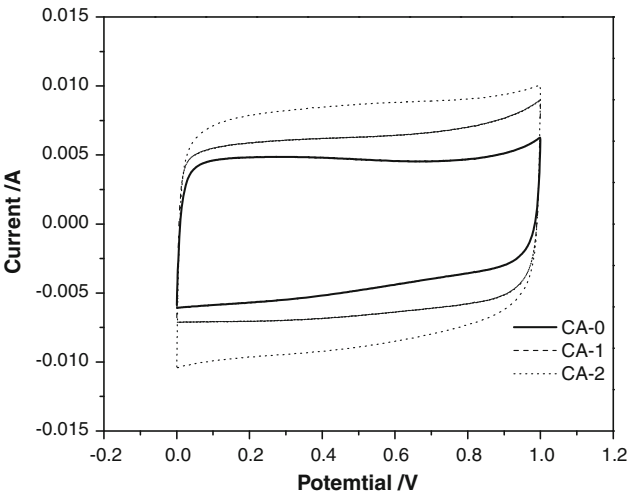

Fig. 9 Cyclic voltammograms of CA-0, CA-1, and CA-2 samples measured at 5 mV s^{-1} in 30% KOH aqueous solution

processes of the electrodes are reversible. The curves maintain nearly rectangular shapes with an increasing voltage sweep rate. This finding is attributed the fact that TiO_2-doped CAs have higher volumes of mesopore than micropore, thus allowing rapid ion transport at a fast sweep rate. The CV curves of samples CA-1, CA-3, and CA-4 are similar to that of sample CA-2. No significant Faradaic reaction was observed during the experiment; hence, the CV behavior represented primarily the EDLC attributed to the electrostatic attractive force of the CA electrodes. Doped TiO_2 in the CA structure was not involved in redox reactions.

The cyclic voltammograms of the CA-0, CA-1, and CA-2 samples measured at 5 mV s^{-1} are displayed in Fig. 9,

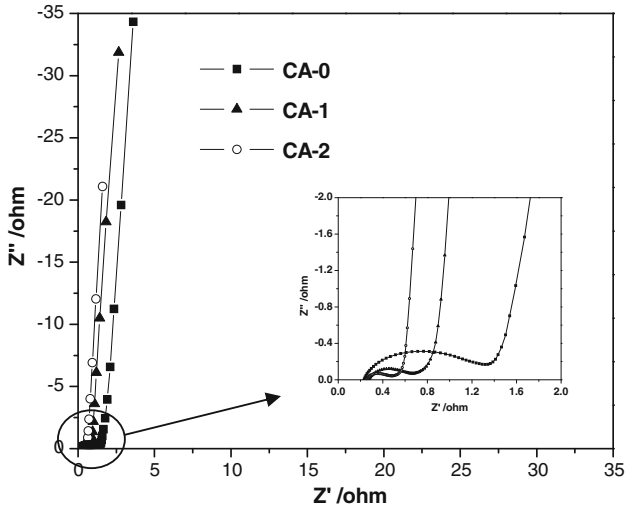

Fig. 10 Impedence plots measured from 50 kHz to 0.01 Hz for the samples CA-0, CA-1, and CA-2

revealing that the capacitance increased with increasing TiO_2 content.

Impedance spectroscopy is a very useful technique for deriving capacitance. The Nyquist plot obtained for the samples (CA-0, CA-1, and CA-2) are described in Fig. 10. The high-frequency arc is ascribed to the charge transfer at the contact interface between the electrode and the electrolyte solution. At the end of the semi-circle arc, a straight line with a slope of 45° from the real axis is observed to correspond to semi-infinite Warburg impedance, which reflects the ion penetration in the thickness of the porous structure of the electrode. In low-frequency regions, all plots show nearly vertical lines, which demonstrate pure capacitance. A decrease in the polarization resistance and Warburg impedance and an enhancement of the capacitive performance can be observed with increasing TiO_2 content. This behavior explains why samples of TiO_2-doped CAs have large numbers of mesopores and average pore size, which facilitates the easy penetration of the ion into the porous structure of the electrode.

The typical constant current charge/discharge curve at a 2 mA cm^{-2} current density for the CA-2 sample is presented in Fig. 11. The curve is almost linear, and a sudden drop in potential at the beginning of charge and discharge is invisible, which shows that the CA electrodes almost do not have internal resistance. The times of charge and discharge are basically the same, indicating that CA electrodes have good reversibility.

To verify the reversibility of the electrode materials, a charge–discharge cycle test was conducted 10,000 times for the CA-2 sample at a 10 mA cm^{-2} current density. From Fig. 12, basically no difference between the 10th cycle and the 10,000th cycle is observed. Figure 13 shows that the decay discharge time is only 8%, whereas the

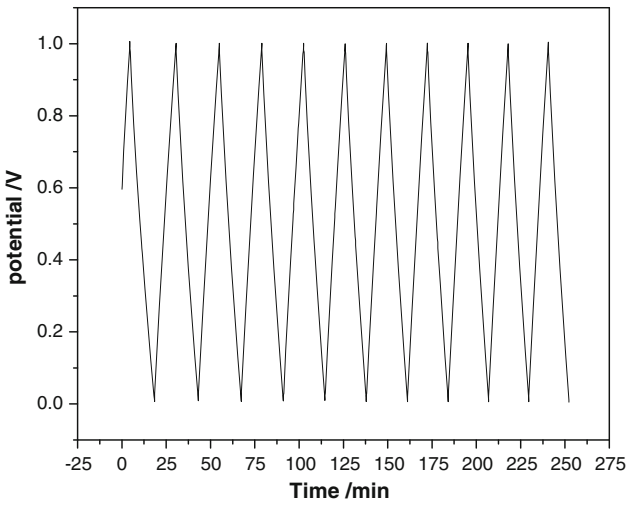

Fig. 11 Typical constant current charge/discharge curves at a current of at 2 mA for the CA-2 sample

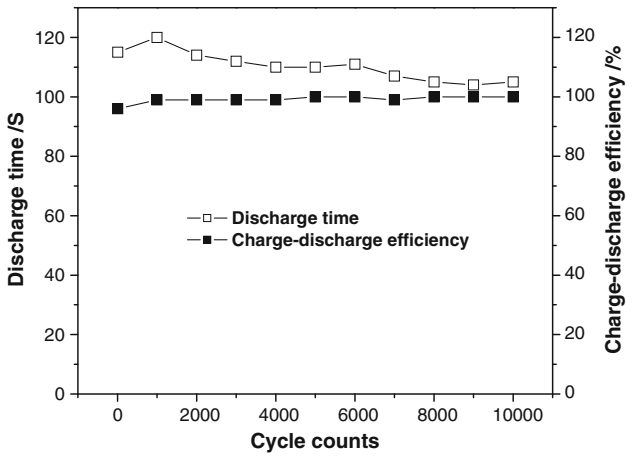

Fig. 13 Discharge time and charge–discharge efficiency curves at a 10 mA current for the CA-2 sample

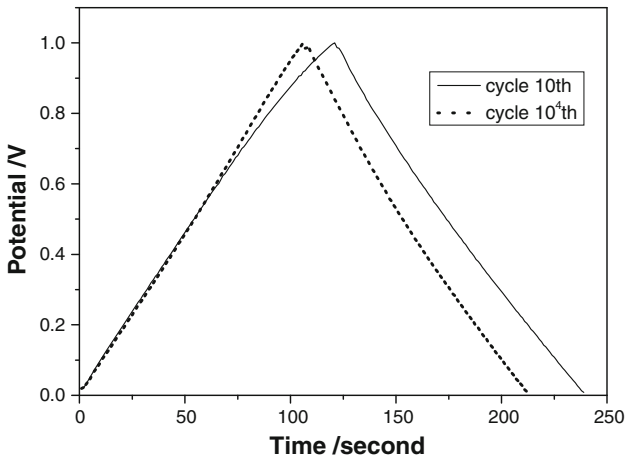

Fig. 12 The 10th cycle charge/discharge curve and the 10,000th cycle curve at a 10 mA current for the CA-2 sample

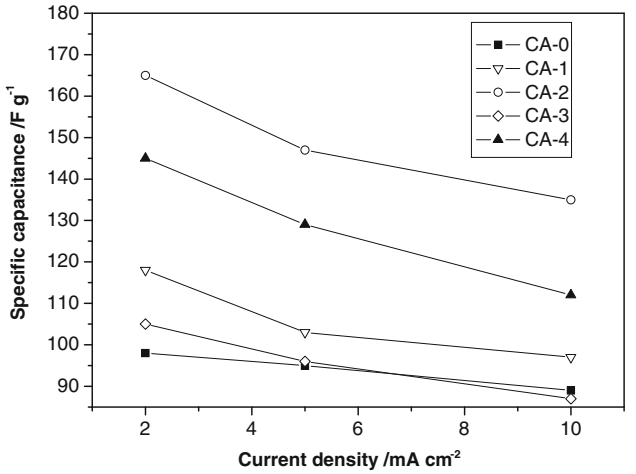

Fig. 14 Variation of the specific capacitance of the carbon aerogels electrodes

charge/discharge efficiency remains at 100% after 10,000 cycles.

The specific capacitance of CAs was calculated according to the formula: $C = 2 \times I \times \Delta t/(m \times \Delta V)$, where m is the mass of CAs in one electrode, I is the current, Δt is the discharge time, and ΔV is the voltage drop. The relevant results are compiled in Fig. 14. The constant current densities applied were 2, 5, and 10 mA cm^{-2}. The capacitance of the CAs is observed to decrease as the applied current increases because the electric double-layer cannot be completely formed at a high current due to a short charge–discharge time.

The specific capacitances of the samples doped by TiO_2 are higher than that of CA-0. Moreover, sample CA-2 has the highest specific capacitance (165 F g^{-1}) among all samples. This finding may be explained by two reasons. One reason is the difference in pore size distribution. The pore and mesopore volumes are increased by the addition of TiO_2, as shown in Table 2. Associating the average pore diameter with the specific capacitances (Fig. 14), these data indicate a direct relationship between the average pore diameter and specific capacitance. Samples with wider pore diameters have higher capacitance values, which could be because a wider pore diameter allows electrolyte ions into more pores. Pore size distribution is believed to be changed by TiO_2 doping; hence, the electrochemical properties are improved. The other reason is the partial graphitization of the CA structure resulting from the addition of TiO_2. Graphitization also increases the electrochemical properties of materials.

4 Conclusions

TiO_2-doped CAs were prepared using the sol–gel synthetic method and supercritical drying process. According to the results on surface area and porosity, the doped TiO_2 has no significant effect on the surface area of the samples, whereas the pore and mesopore volumes are increased by the addition of TiO_2. Particularly, CAs containing 20% TiO_2 significantly increase the average pore size and mesopore volume.

The nature and crystallinity of the particles were also confirmed by the XPS and XRD spectra. Only the anatase phase, rather than a mixture of anatase and rutile, was observed in the samples prepared at 900 °C. TiO_2 incorporation can catalyze the partial graphitization of the CA structure. The TEM results of sample CA-2 indicate that the TiO_2 nanoparticles are well distributed and that the average particle size of TiO_2 is approximately 20 nm.

The TiO_2-doped CAs exhibited an electrical double-layer behavior when used for electrochemical capacitors, and the TiO_2 in the CAs were not involved in redox reactions. The TiO_2-doped CAs had stable electrochemical properties, excellent reversibility, and minimal internal resistance in a 30% KOH aqueous solution. The samples with wider pore diameters have higher capacitance values. The specific capacitance improved to 165 F g^{-1} at 2 mA cm^{-2} current density. Moreover, the charge/discharge efficiency remains at 100% after 10,000 cycles. This study demonstrates that TiO_2-doped CAs are promising materials for supercapacitors.

Acknowledgments It is pleasure to acknowledge the generous financial supports of this research by the National Natural Science Foundation of China (50602003, 50502004) and Beijing Science & Technology star plans (2007B020).

References

1. Kim SJ, Hwang SW, Hyun SH (2005) J Mater Sci 40:725
2. Hwang SW, Hyun SH (2004) J Non-Cryst Solids 347:238
3. Pekala RW, Farmer JC, Alviso CT, Tran TD, Mayer ST, Miller JM, Dunn B (1998) J Non-Cryst Solids 225:74
4. Pekala RW (1989) J Mater Sci 24:3221
5. Pekala RW, Alviso CT, Kong FM, Hulsey SS, Non-Cryst J (1992) Solids 145:90
6. Pekala RW, Kong FM (1989) Rev Phys Appl C4:33
7. Sánchez-Polo M, Rivera-Utrilla J, Salhi E, von Gunten U (2006) J Colloid Interf Sci 300:437
8. Sánchez-Polo M, Rivera-Utrilla J, Salhi E, von Gunten U (2007) Water Res 41:1031
9. Sánchez-Polo M, Rivera-Utrilla J, von Gunten U (2006) Water Res 40:3375
10. Sánchez-Polo M, Rivera-Utrilla J (2006) Appl Cata B: Environ 69:93
11. Sánchez-Polo M, Rivera-Utrilla J, Méndez-Díaz J, López-Penalver J (2008) Ind Eng Chem Res 47:6001
12. Job N, Pirard R, Marien J, Pirard JP (2004) Carbon 42:3217
13. Miller JM, Dunn B (1999) Langmuir 15:799
14. Bekyarova E, Kaneko K (2000) Adv Mater 12:1625
15. Bekyarova E, Kaneko K (1999) Langmuir 15:7119
16. Czakke O, Geissler E, Moussaïd A, Koczka B, László K (2009) Microporous Mesoporous Mater 126:213
17. Czakkel O, Geissler E, Szilágyi IM, Székely E, László K (2009) J Colloid Interf Sci 337:513
18. Maldonado-Hódar FJ, Moreno-Castilla C, Rivera-Utrilla J, Hanzawa Y, Yamada Y (2000) Langmuir 16:4367
19. Maldonado-Hódar FJ, Ferro-García MA, Rivera-Utrilla J, Moreno-Castilla C (1999) Carbon 37:1199
20. Maldonado-Hódar FJ, Pérez-Cadenas AF, Moreno-Castilla C (2003) Carbon 41:1291
21. Moreno-Castilla C, Maldonado-Hódar FJ, Rivera-Utrilla J, Rodríguez-Castellón E (1999) Appl Catal A 183:345
22. Moreno-Castilla C, Maldonado-Hódar FJ, Pérez-Cadenas AF (2003) Langmuir 19:5650
23. Pérez-Cadenas AF, Maldonado-Hódar FJ, Moreno-Castilla C (2005) Langmuir 21:10850
24. Fujishima A, Rao TN, Tryk DA (2000) J Photochem Photobiol C Photochem Rev 1:1
25. Herrmann JM, Disdier J, Pichat P, Malato S, Blanco J (1998) Appl Catal B Environ 17:15
26. Hoffmann MR, Martin ST, Choi W, Bahnemann DW (1995) Chem Rev 95:69
27. Kamat PV (1993) Chem Rev 93:267
28. Kominami H, Murakami S, Kato J, Kera Y, Ohtani B (2002) J Phys Chem B 106:10501
29. Theurich J, Lindner M, Bahnemann DW (1996) Langmuir 12:6368
30. Matos J, Laine J, Herrmann JM (1998) Appl Catal B Environ 18:281
31. Matos J, Laine J, Herrmann JM (1999) Carbon 37:1870
32. Moreno-Castilla C, Maldonado-Hódar FJ, Carrasco-Marín F, Rodríguez-Castellon E (2002) Langmuir 18:2295
33. Ayers MR, Hunt AJ (1998) Mater Lett 34:290
34. Yoganarasimhan SR, Rao CNR (1962) Trans Faraday Soc 58:1579